

The systematic study on the stability and superconductivity of Y-Mg-H compounds under high pressure

Peng Song,¹ Zhufeng Hou,² Pedro Baptista de Castro,^{3,4} Kousuke Nakano,^{1,5} Kenta Hongo,⁶ Yoshihiko Takano,^{3,4} and Ryo Maezono¹

¹School of Information Science, JAIST, Asahidai 1-1, Nomi, Ishikawa 923-1292, Japan

²State Key Laboratory of Structural Chemistry, Fujian Institute of Research on the Structure of Matter, Chinese Academy of Sciences, Fuzhou 350002, China

³National Institute for Materials Science, 1-2-1 Senken, Tsukuba, Ibaraki 305-0047, Japan

⁴University of Tsukuba, 1-1-1 Tennodai, Tsukuba, Ibaraki 305-8577, Japan

⁵International School for Advanced Studies (SISSA), Via Bonomea 265, 34136, Trieste, Italy

⁶Research Center for Advanced Computing Infrastructure, JAIST, Asahidai 1-1, Nomi, Ishikawa 923-1292, Japan

(Dated: July 20, 2021)

Motivated by recent discovery of yttrium-based high-temperature ternary superconducting hydrides (e.g., CaYH₁₂, LaYH₁₂, and ScYH₆), we have employed evolutionary algorithm and first-principles calculations to comprehensively examine the structural stability and superconductivity of the YMgH_x system at high pressure. The hydrogen content x and the pressure are both important factors in the stability of these candidate structures. We find that the stability of hydrogen-rich materials frequently necessitates higher pressure. For instance, the pressures to stabilize $P4/mmm$ -YMgH₈ and $Cmmm$ -YMgH₁₂ are both more than 250 GPa. Hydrogen-less materials, such as $I4_1/amd$ -YMgH₂ and $P6_3/mmc$ -YMgH₃, can be stable at pressures as low as 100 GPa. In addition, we find a metastable structure for YMgH₆ with the same space group as the $P4/mmm$ -YMgH₈. A metastable sodalite-like face-centered cubic (FCC) structure is also found in YMgH₁₂. These four clathrate structures of $P4/mmm$ -YMgH₆, $P4/mmm$ -YMgH₈, $Cmmm$ -YMgH₁₂, and $Fd\bar{3}m$ -YMgH₁₂ is made up of H14, H18, H24, and H24 cages, respectively, in which the H-H pair exhibits weak covalent bonding. According to phonon calculations, $P4/mmm$ -YMgH₆ and $P4/mmm$ -YMgH₈ require a pressure of 300 GPa to maintain dynamic stability, however $Cmmm$ -YMgH₁₂ and $Fd\bar{3}m$ -YMgH₁₂ can maintain dynamic stability at pressures of 200 GPa and 250 GPa, respectively. Electron-phonon coupling calculations indicate that they might be potential high-temperature superconductors, with superconductivity intimately linked to the H cage structure. These clathrate structures exhibit a larger H derived electron density of states at the Fermi level and also a dense H derived phonon density of states. These two portions can interact to generate a greater electron-phonon coupling. Therefore, the sodalite structure $Fd\bar{3}m$ -YMgH₁₂ has a T_c value of 190 K and a strong electron-phonon coupling constant of 2.18.

I. INTRODUCTION

Recently, with the experimental verification of room temperature superconductivity in C-S-H compounds, [1] ternary hydrides have been playing an increasingly important role in the search for novel high-temperature superconductors. However, due to the diversity of ternary hydrides, the difficulty in searching for new superconducting hydrides has increased exponentially, and only about 20 potential superconducting hydrides have been predicted. [1–21] Compared with binary superconducting hydrides, ternary superconducting hydrides have a higher competitive possibility to achieve the room temperature superconductivity. The successful prediction of room temperature superconductor Li₂MgH₁₆ is a good demonstration. [2]

Among the discovered ternary hydrides, they could be classified mainly into three categories. The first category is a combination of metal, non-metal, and hydrogen. In this type of combination, theoretical calculations show the following compounds with superconductivity, such as YSH₆, MgGeH₆, FeSeH₆, CaBH₆, LiBH₂, and so on. [3, 4, 8, 11, 15, 22–25] Interestingly, the introduction of non-metal can reduce the pressure required for stability to a certain extent. For example, LiBH₈ was predicted to have a superconducting transition

temperature (T_c) of 126 K at 50 GPa. [26] Therefore, it is more promising to search for the potential low-pressure-stabilized high-temperature superconductors in these compounds. The second category is a combination of non-metal, non-metal, and hydrogen. In this type of combination, the theoretically predicted superconducting hydrides include H₆SSe, CSH₇, and so on. [5, 8, 17, 27–30] These compounds do not show any particularly obvious structural characteristics. In addition, their phase stability is not high enough. For example, in the CSH₇ reported by Sun and Cui, there may be phase decomposition relative to CH₄ and H₃S. [17, 28] For such compounds, chemical doping may be a more feasible way. [29, 30] For example, in the recently reported C-S-H (287.7 K at 267 GPa), the highest T_c value (270 K) can be achieved when approximately 0.0555 carbon is incorporated into H₃S, as predicted by the virtual crystal approximation (VCA) method. [1, 31] The third category is combinations of metal, metal, and hydrogen. The currently reported potential superconducting compounds with T_c being greater than 200 K mainly fall into such a combination, such as CaYH₁₂, CaMgH₁₂, Li₂MgH₁₆, and so on. [2, 7, 8, 32] Some of these compounds are energetically favorable to form the clathrate structures and also likely to have robust electronic density of states (DOS) at the Fermi level. The structures with robust DOS tend to have a large electron-phonon coupling constant (λ). Generally speaking, larger λ is

easier to show high T_c . [33] For example, the electron-phonon coupling constant of the room temperature superconductor $Fd\bar{3}m$ -Li₂MgH₁₆ can reach an astonishing value of 3.35. [2]

Our target is to search for some compounds with extremely high T_c . Therefore, we pay more attention to the third category of ternary hydrides as mentioned above. Among the binary hydrides discovered, YH₁₀ has the highest T_c value. [34] We first consider the introduction of the second metal element into YH_x. Indeed there have been many reports of potential superconducting hydrides such as ScYH₆, CaYH₁₂, LaYH₁₂, and YKH₁₂. [8, 9, 35–37] In the previous studies of binary hydrides, it has been found that the atomic number, atomic mass, atomic radius, number of electrons, etc., have significant impact on the final T_c value. [38, 39] Lightweight elements usually can have a higher vibration frequency and thus can be helpful to realize a higher T_c value. [33] The superconductivity of hydrides would greatly decrease as the number of *d* electrons and *f* electrons increase. This trend is most obvious in the metal hydrides of the actinides and lanthanides. [39] Considering the atomic mass and the absence of *d* and *f* electrons, Be, Li, Mg, Na, etc. are the most ideal candidate elements to be incorporated into YH_x. Among these candidates, we previously have employed the machine learning method based on the Gradient Boosted Tree (GBT) algorithm to screen which compounds may have extremely high T_c values. [37] For the 1-1-12 composition series compounds, our machine learning predictions show that YMgH₁₂ has the highest T_c value of 198 K among those of the aforementioned four candidate elements. In addition, among the binary hydrides of the aforementioned four candidate elements, MgH₆ has the T_c value (271 K) closest to room temperature. [40]

Therefore, in this rapid communication, we concentrate our attention on introducing Mg into YH_x to study its phase stability and superconductivity under high pressure. In particular, we found that the strong competition between the phase stability and superconductivity of YMgH₆ and that the superconductivity of YMgH_x would depend strongly on the hydrogen content and applied high pressure. More interestingly, we found a metastable phase $Fd\bar{3}m$ -YMgH₁₂ and its superconducting transition temperature could be high up to 190 K at 200 GPa.

II. METHOD

The crystal-structure search for YMgH_x ($x = 2–10, 12, 14$, and 16) at 100, 200, 300 GPa was performed using the US-PEX code. [41] Each structure undergoes 4 steps of relaxation, in which the force on each atom and the stress tensor were optimized using the VASP code [42–45] based on the density functional theory (DFT) within the Perdew-Burke-Ernzerhof (PBE) parameterization [46] of the generalized gradient approximation (GGA). By comparing the relative formation enthalpies on convex hull, the stability of the predicted crystal structure under different pressures is discussed. The electron-phonon coupling spectrum and superconductivity of

these stable structures are calculated by the density functional perturbation theory implemented in the Quantum-ESPRESSO code. [47–49] Regarding the phonon calculations, the structures of YMgH_x with small number of atoms were carried out using the Quantum-ESPRESSO code and the others were performed using the Phonopy [50] code. The details of computational setup in the calculations of phonon, superconductivity, and other properties of different crystal structures of YMgH_x, are given in the Supplemental Material (SM).

III. RESULTS AND DISCUSSION

The pressure-dependent phase diagram of the thermally stabilizing YMgH_x compounds in the pressure range from 100 GPa to 300 GPa is shown in Fig. 1. The pressure-dependent relative enthalpy and thermal convex hull of YMgH_x are given in Figs. S1 and S2 in the SM, respectively. As shown in Fig. S1 in the SM, $I4_1/amd$ -YMgH₂ can be stabilized in a wide pressure range and its decomposition enthalpy indicates that it is stable against $P6/mmm$ -YH₂ [51] and $Im\bar{3}m$ -Mg [52]. Therefore, in the thermal convex hull of YMgH_x we choose $I4_1/amd$ -YMgH₂ and $C2/c$ -H₂ [53] as reference. Herein we predict 10 new stable phases of YMgH_x ($I4_1/amd$ -YMgH₂, $P6_3/mmc$ -YMgH₃, $Pnm2_1$ -YMgH₄, $Imma$ -YMgH₅, $Pmma$ -YMgH₅, $Fmm2$ -YMgH₆, $P2/m$ -YMgH₇, $P4/mmm$ -YMgH₈, $P2_1/m$ -YMgH₉, and $Cmmm$ -YMgH₁₂) and two metastable phases ($P4/mmm$ -YMgH₆ and $Fd\bar{3}m$ -YMgH₁₂). The crystal structures of these predicted new compounds are depicted in Fig. S3 in the SM. Their lattice dynamic stabilities have also been checked by the calculated phonon band structures, which are shown in Figs. S4 and S5 in the SM. From the pressure-dependent phase diagram of YMgH_x, we find that higher pressure is typically required to stabilize the hydrogen-rich materials. To begin with, $I4_1/amd$ -YMgH₂, $P6_3/mmc$ -YMgH₃, $P2/m$ -YMgH₇ all remain thermodynamically stable in the pressure region from 100 GPa to 300 GPa. As seen from the phonon band structures (Figs. S3a, S3b, S4a, and S4b in the SM) of these three materials, we find that $I4_1/amd$ -YMgH₂ and $P6_3/mmc$ -YMgH₃ do not have imaginary frequencies within the studied pressure range, while $P2/m$ -YMgH₇ shows imaginary frequencies from 100 GPa and these imaginary frequencies do not disappear with the increase of pressure. $Pnm2_1$ -YMgH₄ is unstable in the convex hull for the pressure of above 150 GPa. Meanwhile, the calculated relative enthalpy indicates that $Pnm2_1$ -YMgH₄ at 190 GPa may undergo the phase decomposition of $P6/mmm$ -YH₂ [51] + $P6_3/mmc$ -MgH₂ [54]. Phonon calculations show that $Pnm2_1$ -YMgH₄ has imaginary frequencies at 100 GPa, 200 GPa, and 300 GPa, however, these imaginary frequencies are gradually suppressed as the pressure increases. YMgH₅ should undergo a phase transition from $Imma$ to $Pmma$ around 175 GPa. For $Fmm2$ -YMgH₆ and $P4/mmm$ -YMgH₈, they could be stable in the pressure range of 100–150 GPa and 250–300 GPa, respectively. In addition, we also found a metastable structure- $P4/mmm$ in YMgH₆. The enthalpy difference between the metastable $P4/mmm$ phase and the stable $Fmm2$ phase of YMgH₆ at 100 GPa is 0.005 eV/atom. The $P4/mmm$

structure was also found in ScYH_6 and ScCaH_8 . [9, 55] More interestingly, the T_c value of $P4/mmm$ - ScCaH_8 was predicted to be incredibly high up to 212 K. [55] Regarding this context, we are curious to know whether $P4/mmm$ - YMgH_6 and $P4/mmm$ - YMgH_8 would exhibit superconductivity or not, since they possess the same space group as ScCaH_8 . At 200 GPa the phonons of $P4/mmm$ - YMgH_6 and $P4/mmm$ - YMgH_8 show imaginary frequencies, however, at 300 GPa these two phases attain the lattice dynamic stability. In the thermal convex hull diagram, $P2_1/m$ - YMgH_9 could be thermodynamically stabilized in the pressure range of 100-200 GPa, however, its phonons always have imaginary frequencies in such a pressure range. Therefore, the lattice dynamic of $P2_1/m$ - YMgH_9 is unstable. We predicted two highly symmetrical clathrate structures for YMgH_{12} , i.e., the $Cmmm$ phase and the metastable $Fd\bar{3}m$ phase. Their crystal structures are depicted in Fig. 5. These two clathrate structures are composed of H_{24} cages, each with six quadrilaterals and eight hexagons. According to the binary hydrides of Y-H and Mg-H, we analyzed the probable decomposition path of $\text{YH}_6(Im\bar{3}m)$ [51] + $\text{MgH}_2(P6_3/mmc)$ [54] + $2\text{H}_2(C2/c)$ [53] for YMgH_{12} . The calculated results indicate that $Cmmm$ - YMgH_{12} can also be stable over 250 GPa. The calculated phonon dispersion suggests that the lattice dynamics of both the $Cmmm$ and $Fd\bar{3}m$ phases of YMgH_{12} can stay stable over 250 GPa. We should point out that the phases of YMgH_x with $x = 10, 14$, and 16 in the studied pressure range are above the thermodynamic convex hull. In the proceeding subsections we will focus on the thermodynamically stable and metastable phases of YMgH_x with high lattice dynamic stability.

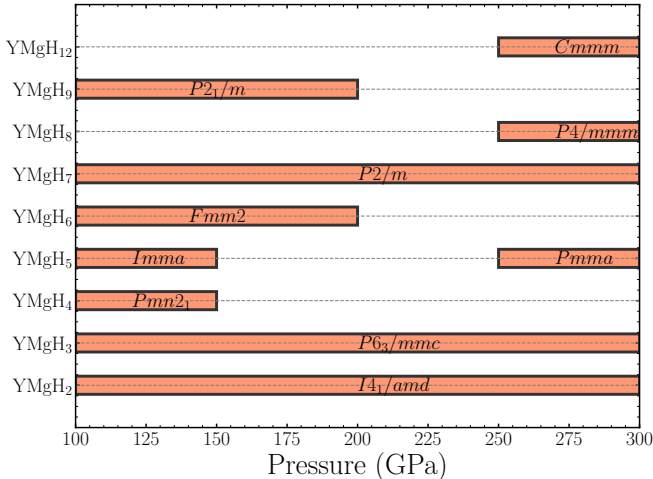


FIG. 1. Pressure-composition phase diagram of YMgH_x .

To discover the superconductivity in YMgH_x , we have calculated the electron-phonon coupling (EPC) spectra of the stable and metastable phases of YMgH_x ($x = 2, 3, 5, 6, 8$, and 12) at certain pressures. The obtained Eliashberg spectral functions of YMgH_x are presented in Fig. S6 in the SM. The predicted T_c values of YMgH_x are summarized in Fig. 3 and also tabulated in Table S2 in the SM. We find that the $I4_1/amd$ -

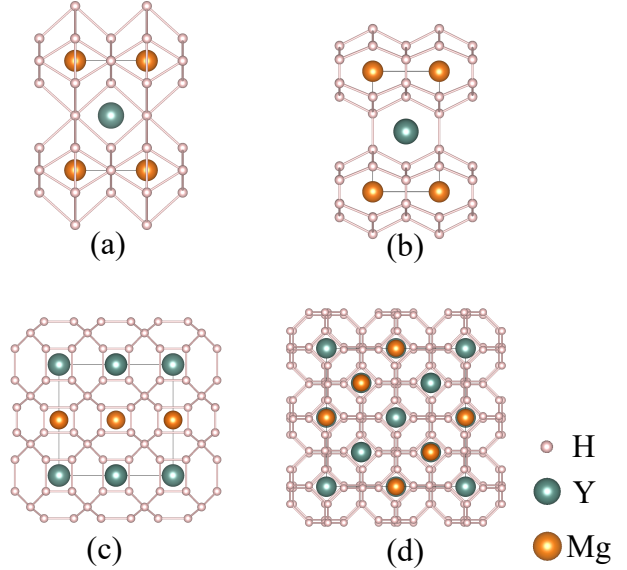


FIG. 2. The clathrate structure of (a) $P4/mmm$ - YMgH_6 , (b) $P4/mmm$ - YMgH_8 , (c) $Cmmm$ - YMgH_{12} , (d) $Fd\bar{3}m$ - YMgH_{12} .

YMgH_2 , $P6_3/mmc$ - YMgH_2 , $Imma$ - YMgH_5 can exhibit superconductivity at high pressure, however, their T_c values at the pressure of 100 GPa are smaller than 2.5 K. For YMgH_5 , the $Pmma$ phase can be stabilized by increasing the pressure (≥ 250 GPa) and the corresponding T_c value is also increased slightly. In particular, the YMgH_x with $x = 6, 8$, and 12 at high pressure exhibit superconductivity with much higher T_c . From the stable $Fmm2$ phase of YMgH_6 to the stable $Cmmm$ phase of YMgH_{12} , the T_c value increases from ~ 31 K (at 120 GPa) to ~ 153 K (at 250 GPa). We also find that the metastable $Fd\bar{3}m$ phase of YMgH_{12} could have a much higher T_c up to about 189 K (at 300 GPa). Therefore, the T_c value of YMgH_x can be boosted by increasing the H content and the pressure.

To understand the trend of the superconductivity in YMgH_x , we have made a close examination of the phonon spectra and electronic structures of YMgH_2 , YMgH_4 , YMgH_5 , YMgH_6 , YMgH_8 , and YMgH_{12} . The corresponding results are presented in Figs. S4, S5, and S7 in the SM. Because of the different mass among Y, Mg, and H atoms, the phonons with lower frequencies ($\lesssim 15$ THz) are dominated by the vibrations of Y and Mg atoms, whereas the high-frequency phonons ($\gtrsim 15$ THz) is contributed by the vibration of H atoms. Generally speaking, the EPC constant λ at the low-frequency region of YMgH_x is rather small, that is to say, the contribution of Y and Mg atoms to the EPC is also small. From YMgH_2 to YMgH_{12} , we find that the high-frequency phonon density of states increase with the increase of H content x . For the $I4_1/amd$ - YMgH_2 , $P6_3/mmc$ - YMgH_3 , and $Imma$ - YMgH_5 , their phonon density of states at the high-frequency region are very small, meanwhile the electronic density of states at the Fermi level (E_F) are also small and contributed dominantly by the Y-4d orbitals, lead-

ing to a rather weak EPC (i.e., $\lambda \lesssim 0.4$). As a result, the T_c values of the $I4_1/amd$ -YMgH₂, $P6_3/mmc$ -YMgH₃, and $Imma$ -YMgH₅ are very small accordingly. Starting with the stable $Fmm2$ phase of YMgH₆, the EPC constant increase dramatically (i.e., nearly doubled). However the electronic states at the E_F of the $Fmm2$ -YMgH₆ is much smaller than those of the metastable $P6/mmm$ -YMgH₆. In the latter case, the contribution of H atoms to the electronic states at the E_F is comparable to that of the Y atom. On the other hand, the metastable $P6/mmm$ -YMgH₆ exhibits stronger EPC than the stable $Fmm2$ -YMgH₆. Therefore, the metastable $P6/mmm$ -YMgH₆ has a higher T_c value. For the $P4/mmm$ -YMgH₈, the vibration of H atoms makes a small contribution to the phonons in the low-frequency range of 0-25 THz, whose dominant contribution comes from the vibration of Y and Mg atoms. Meanwhile the H and Y atoms have almost equal contribution to the electronic states at the E_F of the $P4/mmm$ -YMgH₈. As a result, these features lead to a rather strong EPC (i.e., $\lambda \simeq 1.635$) and a T_c value high up to 124 K for the $P4/mmm$ -YMgH₈. The $Cmmm$ phase of YMgH₁₂ can be stabilized in the pressure from 250 GPa to 300 GPa. It is found that the phonon density of states in the high-frequency range of the $Cmmm$ -YMgH₁₂ increase further as compared with the $P4/mmm$ -YMgH₈, however the former one has a slightly smaller electronic states at the E_F . The EPC constant of $Cmmm$ -YMgH₁₂ is in the same order as the $P4/mmm$ -YMgH₈. For the metastable $Fd\bar{3}m$ -YMgH₁₂, the electronic states at the E_F are slightly larger than those of the stable $Cmmm$ -YMgH₁₂ and its EPC is also stronger than that of the stable $Cmmm$ -YMgH₁₂. Therefore, the metastable $Fd\bar{3}m$ -YMgH₁₂ has a higher T_c value than the stable $Cmmm$ -YMgH₁₂. In both the stable $Cmmm$ and metastable $Fd\bar{3}m$ phases of YMgH₁₂, the contribution of H atoms to the electronic states at the E_F is greater than that of the Y atom. In short, the H content and the weight of H atoms in the electronic states at the E_F play an important role in the superconductivity of YMgH_x.

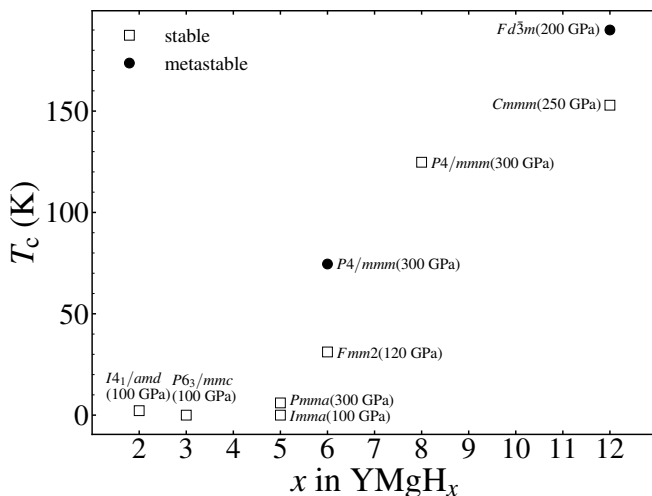


FIG. 3. Calculated superconducting temperature T_c ($\mu = 0.1$) of various structures at high pressure.

The intriguing thing is why the weight of H atoms in the electronic states at the E_F for the hydrogen-rich YMgH_x at high pressure become more significant. Driven by such a question, we carried out the structure analysis and the further examination of the chemical bonding information of the above stable phases. The radial distribution functions of H-H atom pairs in YMgH_x ($x = 2, 3, 4, 5, 6, 8$, and 12) are presented in Fig. S8 in the SM. We find that the first nearest-neighbour distance (1NND) between H atoms in YMgH_x typically decreases as the H content increases. The 1NND of H-H in $P4/mmm$ -YMgH₈ is 0.864 Å, which is very close to the H-H bond length (0.74 Å) of hydrogen molecule. The 1NNDS of H-H in the $Cmmm$ and $Fd\bar{3}m$ phases of YMgH₁₂ are 1.040 and 1.097 Å respectively, which are quite close to those (i.e., 1.19 Å and 1.10 Å) in YH₆ and MgH₆, respectively. [40, 51] This is because the formed clathrate structures of $Cmmm$ -YMgH₁₂ and $Fd\bar{3}m$ -YMgH₁₂ have similarities with MgH₆ and YH₆, namely, they are all composed of H₂₄ cages. The shorter 1NND of H-H indicates that the H atoms may exhibit a molecule-like state to be bonded with the Y and Mg atoms. Generally speaking, if some electrons fill the antibonding state of H₂ molecule, the H-H bond length would be elongated. The slightly elongated 1NNDS of H-H in $P4/mmm$ -YMgH₈, $Cmmm$ -YMgH₁₂, $Fd\bar{3}m$ -YMgH₁₂ than the H-H bond length of H₂ molecule may be partially ascribed to the charge transfer from Y or Mg atoms to the H-H atom pair.

The electron localization function (ELF) of YMgH_x ($x = 6, 8$, and 12) is presented in Fig. 5. The orbital-decomposed density of states and projected crystal orbital Hamilton population (pCOHP) of YMgH_x are presented in Fig. S9 in the SM. The shorter 1NND between H atoms also indicates that the H-H atom pair may form stronger chemical bonding. For instance, the 1NND of H-H in the $I4_1/amd$ -YMgH₂ is about 2.60 Å, which is much larger than that in the $P4/mmm$ -YMgH₆. In the $I4_1/amd$ -YMgH₂ (see Figs. S3a and S9a in the SM), the pCOHP for the first nearest-neighbor (1NN) H-H atom pair is almost zero, indicating no hybridization for them. On the other hand, the H 1s orbital makes a significant contribution to the valence states from -10 eV to -5 eV below the E_F of $I4_1/amd$ -YMgH₂, and it is also hybridized with the Y 4d orbitals and the Mg 3s orbital to form the bonding states. As the H content x in YMgH_x increases, the energy range for the valence states with a significant contribution from the H-1s orbital become wider, which could be associated with the change in the chemical bonding of either the H-H or H-Y. In the $P6_3/mmc$ -YMgH₃, the hybridization between the H-1s orbital and the Y-4d orbitals is greatly enhanced (see Fig. S9b in the SM), while the H-H hybridization is still almost none because the corresponding 1NND is about 1.98 Å. In the $P4/mmm$ -YMgH₈ (see Fig. S9g in the SM), the hybridization between the H-1s orbital and the Y-4d orbitals is further enhanced so that the energy range for the bonding states of H-Y is extended from the E_F to -15 eV, meanwhile the hybridization between the H-H atom pair is also enhanced significantly so that the corresponding states become deeper and to be centered around -15 eV. The anti-bonding states of H-H appear around the E_F of the $P4/mmm$ -YMgH₈. In the

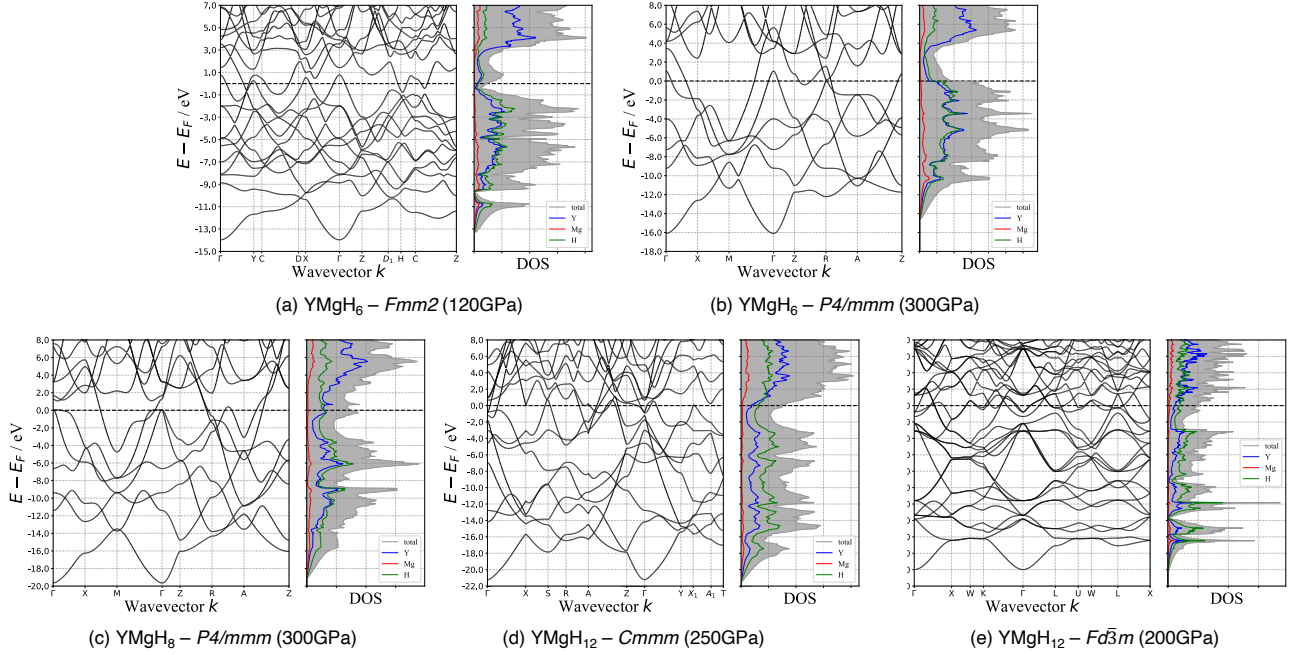


FIG. 4. Electronic band structures and density of states (DOS) for (a) $Fmm2$ - $YMgH_6$ (120 GPa), (b) $P4/mmm$ - $YMgH_6$ (300 GPa), (c) $P4/mmm$ - $YMgH_8$ (300 GPa), (d) $Cmmm$ - $YMgH_{12}$ (250 GPa), and (e) $Fd\bar{3}m$ - $YMgH_{12}$ (200 GPa).

$Cmmm$ - $YMgH_{12}$ and $Fd\bar{3}m$ - $YMgH_{12}$ the anti-bonding states of H-H appear just below the E_F (see Figs. S9h and S9i in the SM). Therefore, the H-H atom pair forms strong covalent bonding. This also can be seen from the ELF, as shown in Fig. 5d. From the analysis of DOS of $YMgH_x$, we find that the contribution of H-1s electrons to the electronic states at the E_F tends to increase as the H content x increases. For the $I4_1/amd$ - $YMgH_2$ and $P6_3/mmc$ - $YMgH_3$, the states at the E_F are dominated by the Y-4d orbitals and the contribution other orbital could be negligible. For the $Pmma$ - $YMgH_5$, $YMgH_6$, $YMgH_8$, and $YMgH_{12}$, the contribution of the H atoms to the states at the E_F become more robust and is comparable to the contribution of the Y-4d orbitals. This is due to the filling of anti-bonding states of H-H atom pair by the electron transferred from metal atoms.

IV. CONCLUSION

In summary, we systematically investigated the stability and superconductivity of the ternary hydride $YMgH_x$ at high pressure. For $YMgH_x$ with $x = 6, 8$, and 12 , they thermodynamically prefer to take the clathrate structure composed of H_{14} , H_{18} , and H_{24} cages, respectively, in which strong covalent connections between H-H can be formed. According to the EPC calculations, these clathrate structures of $YMgH_x$ all can exhibit high-temperature superconductivity. The interplay of the extraordinarily high weight in the electronic density of states at the Fermi level and the dense phonon

density of states associated with H atoms in these clathrate structures of $YMgH_x$ results in a significant electron-phonon coupling. The $Fd\bar{3}m$ - $YMgH_{12}$, a metastable sodalite structure, exhibits a T_c of up to 190 K at 200 GPa. The cage structure of the superconducting ternary hydride resembles that of the superconducting binary hydride in a similar way. For example, H_{18} cages are also present in both $I4/mmm$ - YH_4 [51] and $P4/mmm$ - $YMgH_8$. H_{24} cages are also found in MgH_6 [40], $Im\bar{3}m$ - YH_6 [34], $Cmmm$ - $YMgH_{12}$, and $Fd\bar{3}m$ - $YMgH_{12}$. These results suggest that the search for new potential high-temperature superconducting ternary hydrides can be substantially accelerated by starting with the structure of the superconducting binary clathrates.

V. ACKNOWLEDGMENTS

The computations in this work have been performed using the facilities of Research Center for Advanced Computing Infrastructure (RCACI) at JAIST. K.H. is grateful for financial support from the HPCI System Research Project (Project ID: hp190169) and MEXT-KAKENHI (JP16H06439, JP17K17762, JP19K05029, and JP19H05169). R.M. is grateful for financial supports from MEXT-KAKENHI (19H04692 and 16KK0097), FLAGSHIP2020 (project nos. hp190169 and hp190167 at K-computer), Toyota Motor Corporation, I-O DATA Foundation, the Air Force Office of Scientific Research (AFOSR-AOARD/FA2386-17-1-4049;FA2386-19-1-4015), and JSPS Bilateral Joint Projects

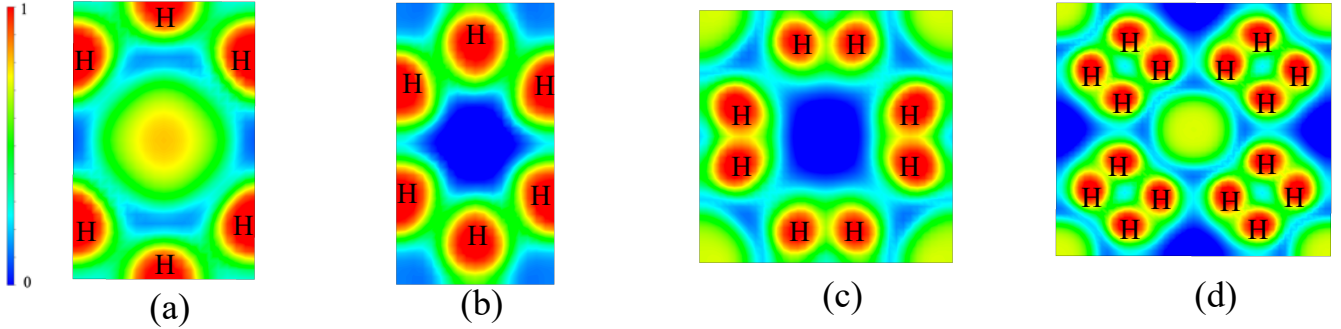


FIG. 5. The contour plots of electron localization function (ELF) on (a) (200) plane of $P4/mmm$ -YMgH₆, (b) (200) plane of $P4/mmm$ -YMgH₈, (c) (100) plane of $Cmmm$ -YMgH₈, and (d) (100) plane of $Fd\bar{3}m$ -YMgH₁₂

(with India DST).

-
- [1] E. Snider, N. Dasenbrock-Gammon, R. McBride, M. Debessai, H. Vindana, K. Vencatasamy, K. V. Lawler, A. Salamat, and R. P. Dias, *Nature* **586**, 373 (2020).
- [2] Y. Sun, J. Lv, Y. Xie, H. Liu, and Y. Ma, *Phys. Rev. Lett.* **123**, 097001 (2019).
- [3] Y. Ma, D. Duan, Z. Shao, H. Yu, H. Liu, F. Tian, X. Huang, D. Li, B. Liu, and T. Cui, *Phys. Rev. B* **96**, 144518 (2017).
- [4] Y. Ma, D. Duan, Z. Shao, D. Li, L. Wang, H. Yu, F. Tian, H. Xie, B. Liu, and T. Cui, *Phys. Chem. Chem. Phys.* **19**, 27406 (2017).
- [5] D. Li, Y. Liu, F.-B. Tian, S.-L. Wei, Z. Liu, D.-F. Duan, B.-B. Liu, and T. Cui, *Front. Phys.* **13**, 137107 (2018).
- [6] X. Liang, S. Zhao, C. Shao, A. Bergara, H. Liu, L. Wang, R. Sun, Y. Zhang, Y. Gao, Z. Zhao, X.-F. Zhou, J. He, D. Yu, G. Gao, and Y. Tian, *Phys. Rev. B* **100**, 184502 (2019).
- [7] M. Rahm, R. Hoffmann, and N. W. Ashcroft, *J. Am. Chem. Soc.* **139**, 8740 (2017).
- [8] X. Liang, A. Bergara, L. Wang, B. Wen, Z. Zhao, X.-F. Zhou, J. He, G. Gao, and Y. Tian, *Phys. Rev. B* **99**, 100505 (2019).
- [9] Y. K. Wei, L. Q. Jia, Y. Y. Fang, L. J. Wang, Z. X. Qian, J. N. Yuan, G. Selvaraj, G. F. Ji, and D. Q. Wei, *Int. J. Quantum Chem.* **121**, e26459 (2020).
- [10] H. Xie, D. Duan, Z. Shao, H. Song, Y. Wang, X. Xiao, D. Li, F. Tian, B. Liu, and T. Cui, *J. Phys.: Condens. Matter* **31**, 245404 (2019).
- [11] C. Kokail, W. von der Linden, and L. Boeri, *Phys. Rev. Materials* **1**, 074803 (2017).
- [12] Z. Shao, D. Duan, Y. Ma, H. Yu, H. Song, H. Xie, D. Li, F. Tian, B. Liu, and T. Cui, *npj Comput. Mater.* **5**, 1 (2019).
- [13] J. Zhang, J. M. McMahon, A. R. Oganov, X. Li, X. Dong, H. Dong, and S. Wang, *Phys. Rev. B* **101**, 134108 (2020).
- [14] P. Zhang, Y. Sun, X. Li, J. Lv, and H. Liu, *Phys. Rev. B* **102**, 184103 (2020).
- [15] S. D. Cataldo, W. von der Linden, and L. Boeri, *Phys. Rev. B* **102**, 014516 (2020).
- [16] X. Guo, R.-L. Wang, H.-L. Chen, W.-C. Lu, K. Ho, and C. Wang, *Phys. Lett. A* **384**, 126189 (2020).
- [17] W. Cui, T. Bi, J. Shi, Y. Li, H. Liu, E. Zurek, and R. J. Hemley, *Phys. Rev. B* **101**, 134504 (2020).
- [18] H.-Y. Lv, S.-Y. Zhang, M.-H. Li, Y.-L. Hai, N. Lu, W.-J. Li, and G.-H. Zhong, *Phys. Chem. Chem. Phys.* **22**, 1069 (2020).
- [19] Y. Yan, T. Bi, N. Geng, X. Wang, and E. Zurek, *J. Phys. Chem. Lett.* **11**, 9629 (2020).
- [20] T. Muramatsu, W. K. Wanene, M. Somayazulu, E. Vinitsky, D. Chandra, T. A. Strobel, V. V. Struzhkin, and R. J. Hemley, *J. Phys. Chem. C* **119**, 18007 (2015).
- [21] D. Meng, M. Sakata, K. Shimizu, Y. Iijima, H. Saitoh, T. Sato, S. Takagi, and S. ichi Orimo, *Phys. Rev. B* **99**, 024508 (2019).
- [22] J. Chen, X. Xue, H. Chen, H. Liu, Q. Zang, and W. Lu, *J. Phys. Chem. C* **123**, 28008 (2019).
- [23] K. S. Grishakov, N. N. Degtyarenko, and E. A. Mazur, *J. Phys.: Conf. Ser.* **1238**, 012017 (2019).
- [24] X. Li, Y. Xie, Y. Sun, P. Huang, H. Liu, C. Chen, and Y. Ma, *J. Phys. Chem. Lett.* **11**, 935 (2020).
- [25] L. Hao, Z. Yuan, X. Guo, Y. Zhang, K. Luo, Y. Gao, F. Ling, X. Chen, Z. Zhao, and D. Yu, *Phys. Lett. A* **384**, 126525 (2020).
- [26] S. Di Cataldo, C. Heil, W. von der Linden, and L. Boeri, *arXiv preprint arXiv:2102.11227* (2021).
- [27] B. Liu, W. Cui, J. Shi, L. Zhu, J. Chen, S. Lin, R. Su, J. Ma, K. Yang, M. Xu, J. Hao, A. P. Durajski, J. Qi, Y. Li, and Y. Li, *Phys. Rev. B* **98**, 174101 (2018).
- [28] Y. Sun, Y. Tian, B. Jiang, X. Li, H. Li, T. Iitaka, X. Zhong, and Y. Xie, *Phys. Rev. B* **101**, 174102 (2020).
- [29] P.-H. Chang, S. Silayi, D. Papaconstantopoulos, and M. Mehl, *J. Phys. Chem. Solids* **139**, 109315 (2020).
- [30] A. Nakanishi, T. Ishikawa, and K. Shimizu, *J. Phys. Soc. Jpn.* **87**, 124711 (2018).
- [31] T. Wang, M. Hirayama, T. Nomoto, T. Koretsune, R. Arita, and J. A. Flores-Livas, *arXiv preprint arXiv:2104.03710* (2021).
- [32] W. Sukmas, P. Tsuppayakorn-aek, U. Pinsook, and T. Bovornratanaraks, *J. Alloy Compd.* **849**, 156434 (2020).
- [33] N. W. Ashcroft, *Phys. Rev. Lett.* **92**, 187002 (2004).
- [34] C. Heil, S. di Cataldo, G. B. Bachelet, and L. Boeri, *Phys. Rev. B* **99**, 220502 (2019).
- [35] D. V. Semenok, I. A. Troyan, A. G. Kvashnin, A. G. Ivanova, M. Hanfland, A. V. Sadakov, O. A. Sobolevskiy, K. S. Perovakov, A. G. Gavriluk, I. S. Lyubutin, *et al.*, *arXiv preprint arXiv:2012.04787* (2020), 10.1016/j.mattod.2021.03.025.

- [36] P. Song, Z. Hou, P. B. de Castro, K. Nakano, K. Hongo, Y. Takano, and R. Maezono, *arXiv preprint arXiv:2103.06690* (2021).
- [37] P. Song, Z. Hou, P. B. de Castro, K. Nakano, K. Hongo, Y. Takano, and R. Maezono, *arXiv preprint arXiv:2103.00193* (2021).
- [38] J. A. Flores-Livas, L. Boeri, A. Sanna, G. Profeta, R. Arita, and M. Eremets, *Physics Reports* **856**, 1 (2020).
- [39] D. V. Semenok, I. A. Kruglov, I. A. Savkin, A. G. Kvashnin, and A. R. Oganov, *Current Opinion in Solid State and Materials Science* **24**, 100808 (2020).
- [40] X. Feng, J. Zhang, G. Gao, H. Liu, and H. Wang, *RSC Adv.* **5**, 59292 (2015).
- [41] C. W. Glass, A. R. Oganov, and N. Hansen, *Comput. Phys. Commun.* **175**, 713 (2006).
- [42] G. Kresse and J. Hafner, *Phys. Rev. B* **47**, 558 (1993).
- [43] G. Kresse and J. Hafner, *Phys. Rev. B* **49**, 14251 (1994).
- [44] G. Kresse and J. Furthmüller, *Comput. Mater. Sci.* **6**, 15 (1996).
- [45] G. Kresse and J. Furthmüller, *Phys. Rev. B* **54**, 11169 (1996).
- [46] J. P. Perdew, K. Burke, and M. Ernzerhof, *Phys. Rev. Lett.* **77**, 3865 (1996).
- [47] P. Giannozzi, S. Baroni, N. Bonini, M. Calandra, R. Car, C. Cavazzoni, D. Ceresoli, G. L. Chiarotti, M. Cococcioni, I. Dabo, A. D. Corso, S. de Gironcoli, S. Fabris, G. Fratesi, R. Gebauer, U. Gerstmann, C. Gougaussis, A. Kokalj, M. Lazzeri, L. Martin-Samos, N. Marzari, F. Mauri, R. Mazzarello, S. Paolini, A. Pasquarello, L. Paulatto, C. Sbraccia, S. Scandolo, G. Sclauzero, A. P. Seitsonen, A. Smogunov, P. Umari, and R. M. Wentzcovitch, *J. Phys.: Condens. Matter* **21**, 395502 (2009).
- [48] P. Giannozzi, O. Andreussi, T. Brumme, O. Bunau, M. B. Nardelli, M. Calandra, R. Car, C. Cavazzoni, D. Ceresoli, M. Cococcioni, N. Colonna, I. Carnimeo, A. D. Corso, S. de Gironcoli, P. Delugas, R. A. DiStasio, A. Ferretti, A. Floris, G. Fratesi, G. Fugallo, R. Gebauer, U. Gerstmann, F. Giustino, T. Gorni, J. Jia, M. Kawamura, H.-Y. Ko, A. Kokalj, E. Küçükbenli, M. Lazzeri, M. Marsili, N. Marzari, F. Mauri, N. L. Nguyen, H.-V. Nguyen, A. O. de-la Roza, L. Paulatto, S. Poncé, D. Rocca, R. Sabatini, B. Santra, M. Schlipf, A. P. Seitsonen, A. Smogunov, I. Timrov, T. Thonhauser, P. Umari, N. Vast, X. Wu, and S. Baroni, *J. Phys.: Condens. Matter* **29**, 465901 (2017).
- [49] P. Giannozzi, O. Baseggio, P. Bonfà, D. Brunato, R. Car, I. Carnimeo, C. Cavazzoni, S. de Gironcoli, P. Delugas, F. F. Ruffino, A. Ferretti, N. Marzari, I. Timrov, A. Urru, and S. Baroni, *J. Chem. Phys.* **152**, 154105 (2020).
- [50] A. Togo and I. Tanaka, *Scripta Mater.* **108**, 1 (2015).
- [51] H. Liu, I. I. Naumov, R. Hoffmann, N. W. Ashcroft, and R. J. Hemley, *Proc. Natl. Acad. Sci. USA* **114**, 6990 (2017).
- [52] Q. Liu, C. Fan, and R. Zhang, *J. Appl. Phys.* **105**, 123505 (2009).
- [53] C. J. Pickard and R. J. Needs, *Nature Phys.* **3**, 473 (2007).
- [54] P. Vajeeston, P. Ravindran, B. C. Hauback, H. Fjellvåg, A. Kjekshus, S. Furuseth, and M. Hanfland, *Phys. Rev. B* **73**, 224102 (2006).
- [55] L.-T. Shi, Y.-K. Wei, A.-K. Liang, R. Turnbull, C. Cheng, X.-R. Chen, and G.-F. Ji, *J. Mater. Chem. C* **9**, 7284 (2021).

Supplemental Material

for

The systematic study on the stability and superconductivity of Y-Mg-H compounds under high pressure

Peng Song,¹ Zhufeng Hou,² Pedro Baptista de Castro,^{3,4} Kousuke Nakano,^{1,5} Kenta Hongo,⁶ Yoshihiko Takano,^{3,4} and Ryo Maezono¹

¹*School of Information Science, JAIST, Asahidai 1-1, Nomi, Ishikawa 923-1292, Japan*

²*State Key Laboratory of Structural Chemistry, Fujian Institute of Research on the Structure of Matter, Chinese Academy of Sciences, Fuzhou 350002, China*

³*National Institute for Materials Science, I-2-1 Sengen, Tsukuba, Ibaraki 305-0047, Japan*

⁴*University of Tsukuba, I-1-1 Tennodai, Tsukuba, Ibaraki 305-8577, Japan*

⁵*International School for Advanced Studies (SISSA), Via Bonomea 265, 34136, Trieste, Italy*

⁶*Research Center for Advanced Computing Infrastructure, JAIST, Asahidai 1-1, Nomi, Ishikawa 923-1292, Japan*

A. Computational details

The crystal structure prediction for YMgH_x ($x = 2\text{-}10, 12, 14$, and 16) at the high pressure ranging from 100 GPa to 300 GPa were carried out using the USPEX (Universal Structure Predictor: Evolutionary Xtallography)¹ code combined with the VASP (Vienna *ab initio* simulation package)^{2–5} code. These chemical compositions are created at random, with the first 400 structures being created at random, and each subsequent generation producing 100 structures. These structures are composed of 40% heredity, 40% random, 10% mutation, and 10% soft mutation. The energy of the produced structures is minimized globally using Perdew-Burke-Ernzerhof (GGA-PBE)⁶ through three DFT computations. We choose around ten of the structures with the lowest structural energy for each chemical composition and undertake two higher-precision optimizations to guarantee that they can converge well under 1 meV. Finally, the structure with the lowest energy is chosen as the final contender among these structures. The LOBSTER algorithm is used to compute the output result coupled with VASP for the crystal orbital Hamiltonian population (COHP) and the integrated crystal orbital Hamiltonian population (ICOHP).^{2–5,7} The supercell method, as implemented in the Phonopy code,⁸ was used to calculate phonons for YMgH₄, YMgH₇, and YMgH₉. Quantum ESPRESSO is used to compute the phonons of YMgH₂, YMgH₃, YMgH₅, YMgH₆, YMgH₈, and YMgH₁₂.^{9–11} The electron-phonon coupling (EPC) constant λ of these stable compounds was calculated by quantum ESPRESSO with a plane wave basis set up to a cutoff energy of 60 Ry and Marzari-Vanderbilt method in the context of linear response theory. The EPC calculation matrix is shown in Table S1. The superconducting transition temperature T_c is calculated using McMillan's equation.¹²

$$T_c = \frac{\Theta}{1.45} \exp\left[-\frac{1.04(1 + \lambda)}{\lambda - \mu^*(1 + 0.62\lambda)}\right] \quad (\text{S1})$$

where Θ is the Debye temperature of the system. $\Theta = \frac{1.45}{1.2} \omega_{\log}$. This ω_{\log} is the logarithmic average of the spectral function, which was introduced by Dynes.

TABLE S1: The setup of k -point mesh in the self-consistent field (SCF) calculations and of q -point mesh in the phonon calculations.

Compound	<i>I4₁/amd</i> -YMgH ₂	<i>P6₃/mmc</i> -YMgH ₃	<i>Imma</i> -YMgH ₅	<i>Pmma</i> -YMgH ₅	<i>Fmm2</i> -YMgH ₆	<i>P4/mmm</i> -YMgH ₆
SCF dense k -point	$12 \times 12 \times 12$	$16 \times 16 \times 8$	$12 \times 12 \times 12$	$12 \times 12 \times 12$	$12 \times 12 \times 12$	$16 \times 16 \times 12$
phonon q -kpoint	$3 \times 3 \times 3$	$4 \times 4 \times 2$	$3 \times 3 \times 3$	$3 \times 3 \times 3$	$3 \times 3 \times 3$	$4 \times 4 \times 3$
Compound	<i>P4/mmm</i> -YMgH ₈	<i>Cmmm</i> -YMgH ₁₂	<i>Fd\bar{3}m</i> -YMgH ₁₂			
SCF dense k -point	$16 \times 16 \times 12$	$16 \times 16 \times 12$	$16 \times 16 \times 16$			
phonon q -kpoint	$4 \times 4 \times 3$	$4 \times 4 \times 3$	$4 \times 4 \times 4$			

B. Supplementary figures

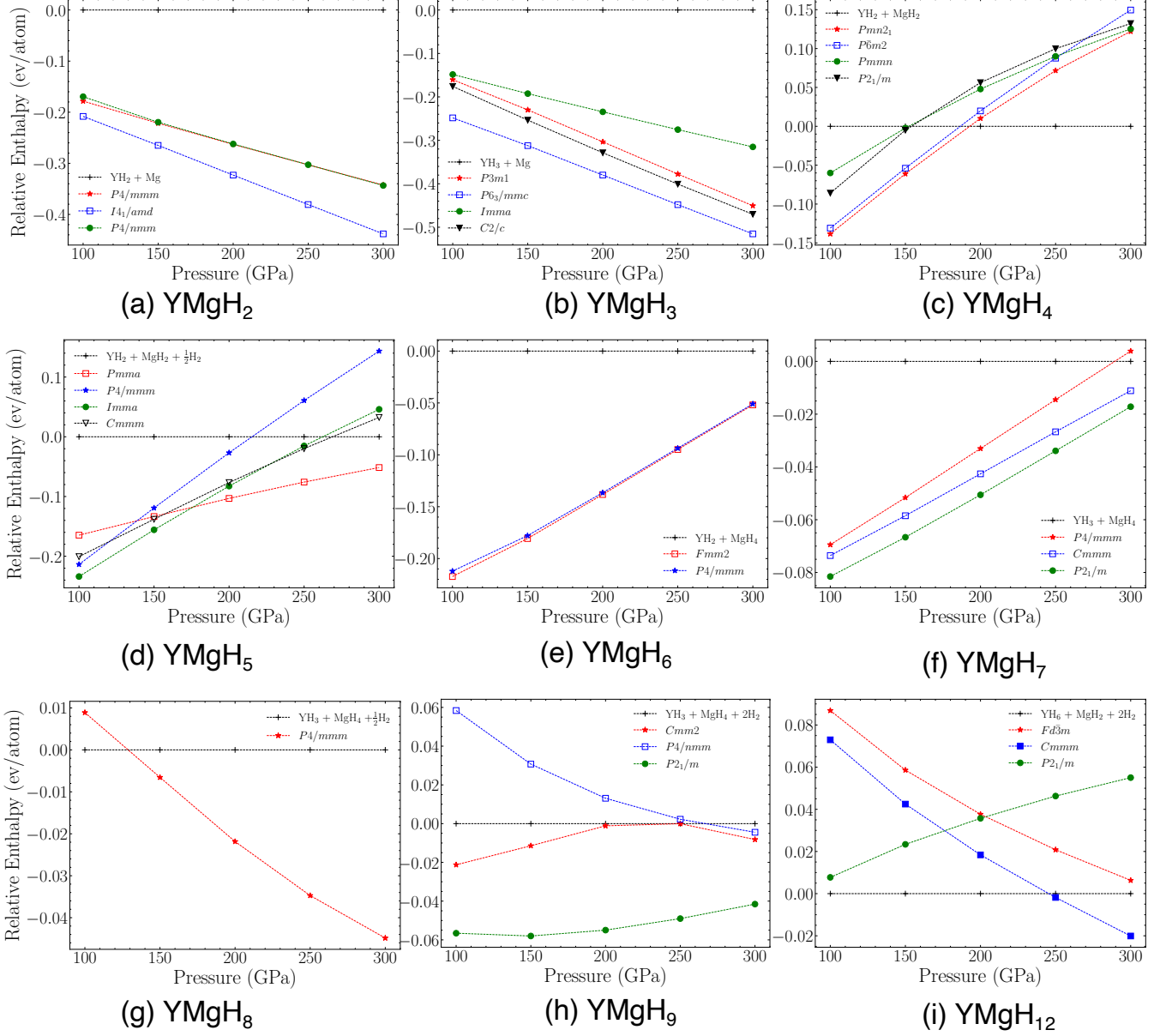


FIG. S1: Comparisons of enthalpies among the candidate structures for the YMgH_x at the pressure ranging from 100 GPa to 300 GPa. The decomposition enthalpy is compared with H₂, ¹³ Mg, ¹⁴ MgH₂, ¹⁵ MgH₄, ¹⁵ YH₂, ¹⁶ YH₃, ¹⁶ YH₄, ¹⁶ and YH₆. ¹⁶

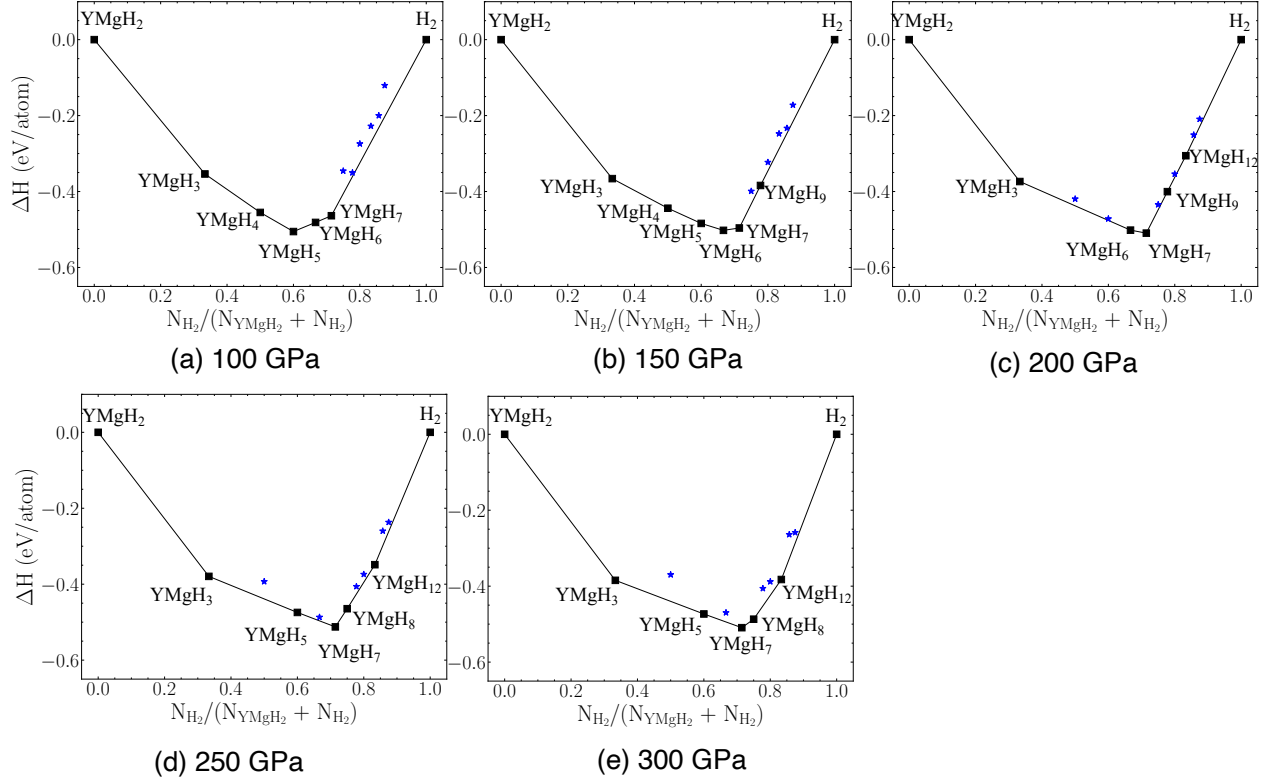


FIG. S2: Convex hull of YMgH_x relative to YMgH_2 and $\text{H}-\text{C}2/c^{13}$ at the pressure of (a) 100 GPa, (b) 150 GPa, (c) 200GPa, (d) 250 GPa, and (e) 300 GPa.

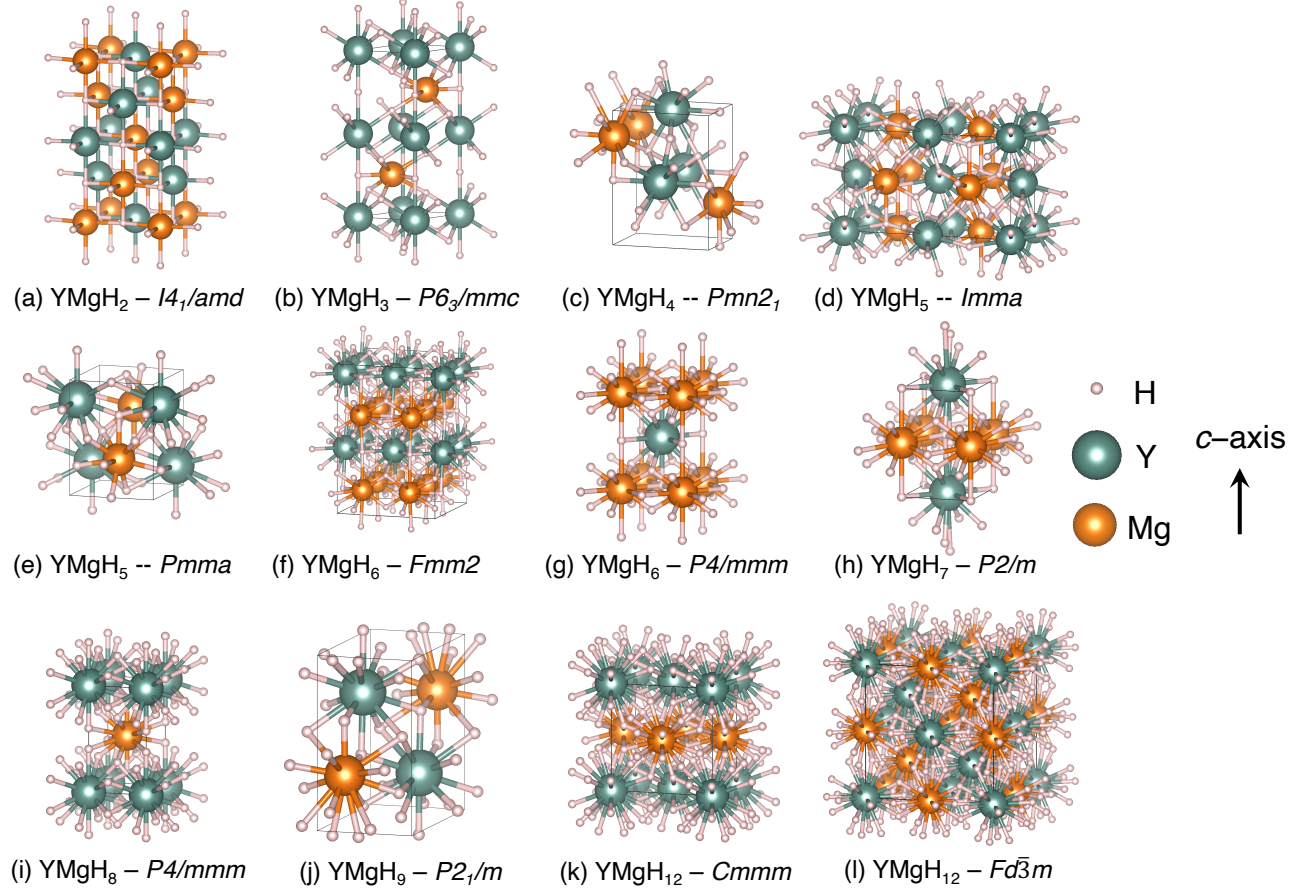


FIG. S3: Crystal structures of the predicted YMgH_x phases.

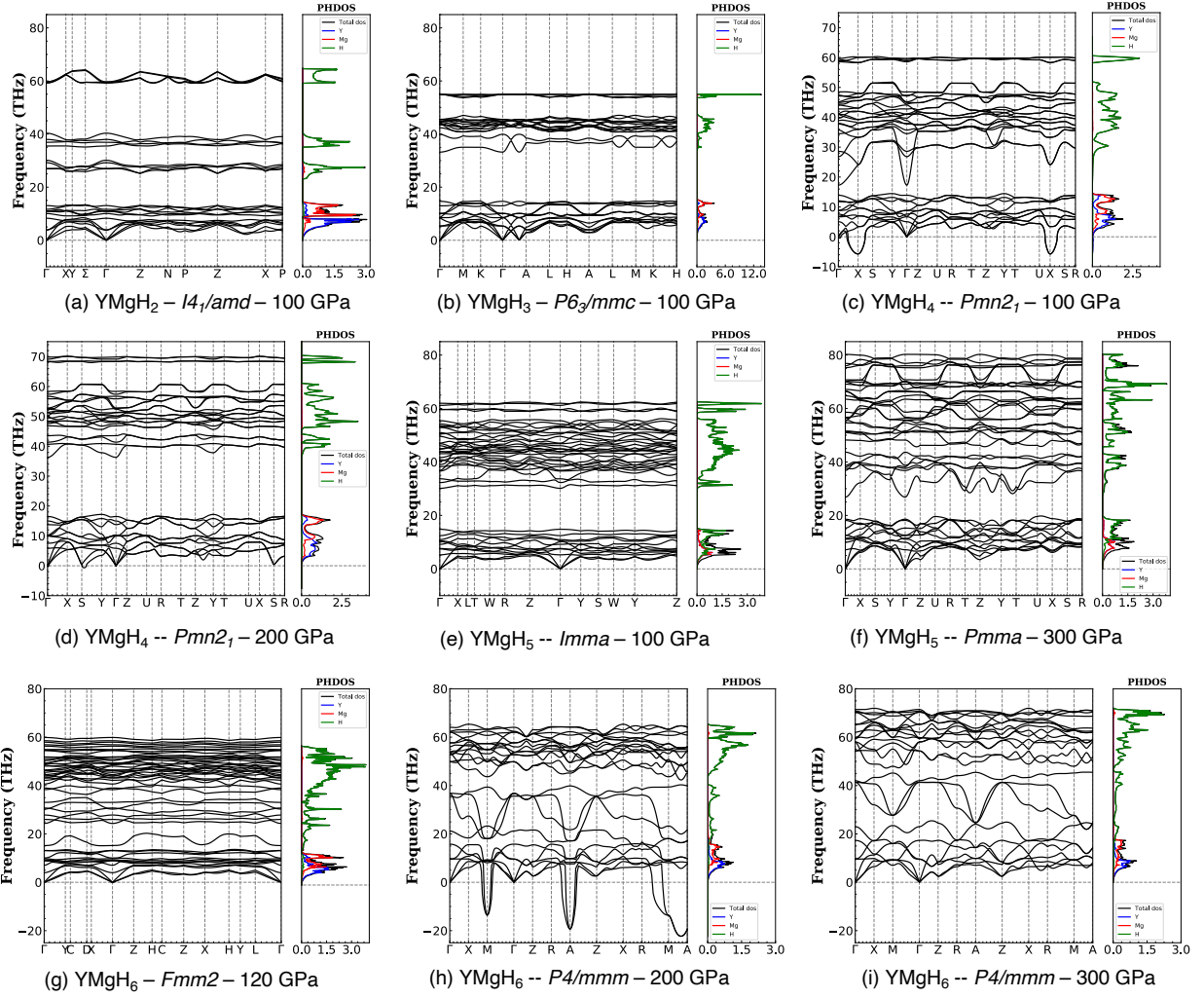


FIG. S4: Phonon band structures and atom-projected phonon density of states of (a) YMgH₂- $I4_1/AMD$ at 100 GPa, (b) YMgH₃- $P6_3/MMC$ at 100 GPa, (c) YMgH₄- $Pmn2_1$ at 100 GPa, (d) YMgH₄- $Pmn2_1$ at 200 GPa, (e) YMgH₅- $Imma$ at 100 GPa, (f) YMgH₅- $Pmma$ at 300 GPa, (g) YMgH₆- $Fmm2$ at 120 GPa, (h) YMgH₆- $P4/mmm$ at 200 GPa, and (i) YMgH₆- $P4/mmm$ at 300 GPa.

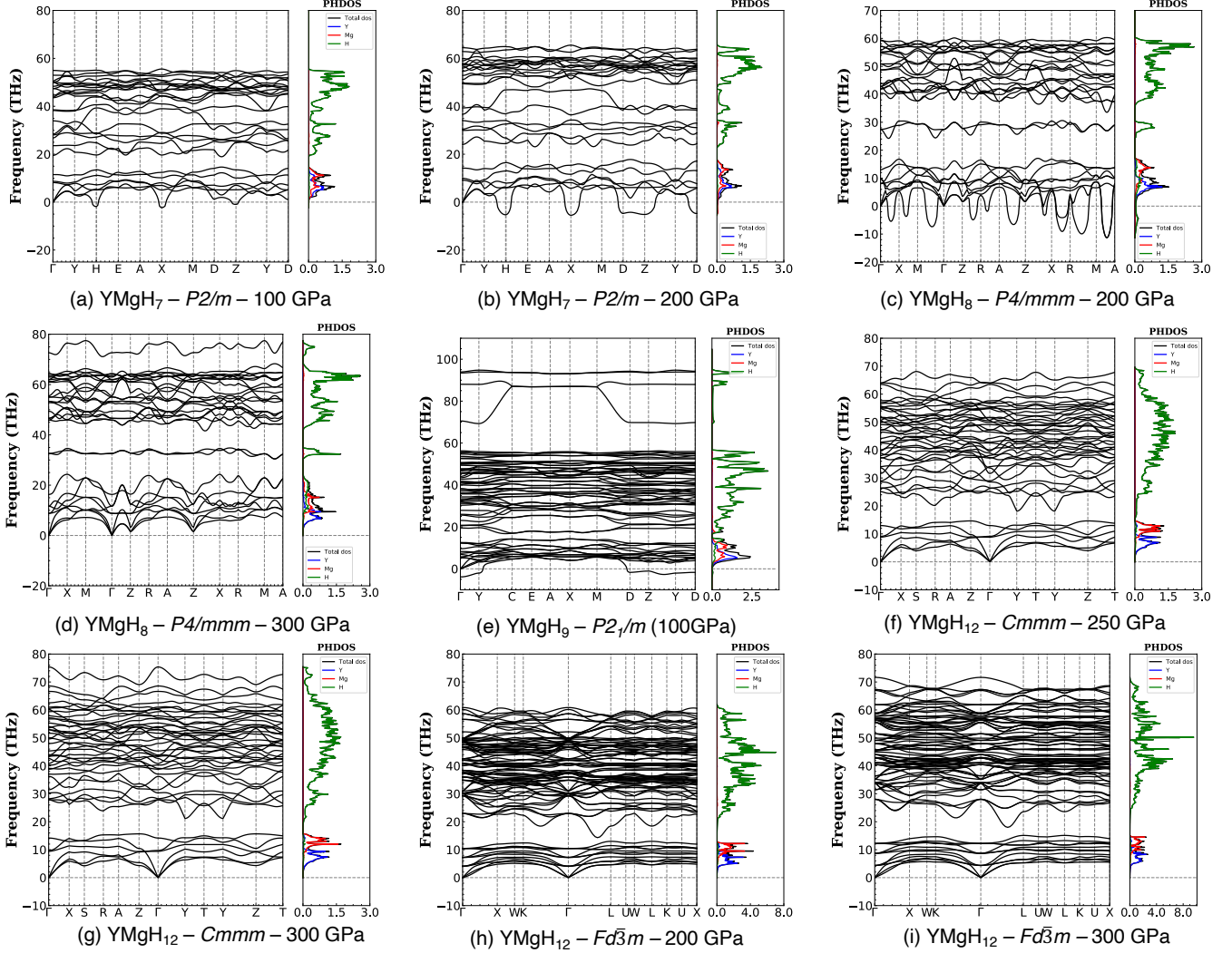


FIG. S5: Phonon band structures and atom-projected phonon density of states of (a) YMgH₇– $P2/m$ at 100 GPa, (b) YMgH₇– $P2/m$ at 200 GPa, (c) YMgH₈– $P4/mmm$ at 200 GPa, (d) YMgH₈– $P4/mmm$ at 300 GPa, (e) YMgH₉– $P2_1/m$ at 100 GPa, (f) YMgH₁₂– $Cmmm$ at 250 GPa, (g) YMgH₁₂– $Cmmm$ at 300 GPa, (h) YMgH₁₂– $Fd\bar{3}m$ at 200 GPa, and (i) YMgH₁₂– $Fd\bar{3}m$ at 300 GPa.

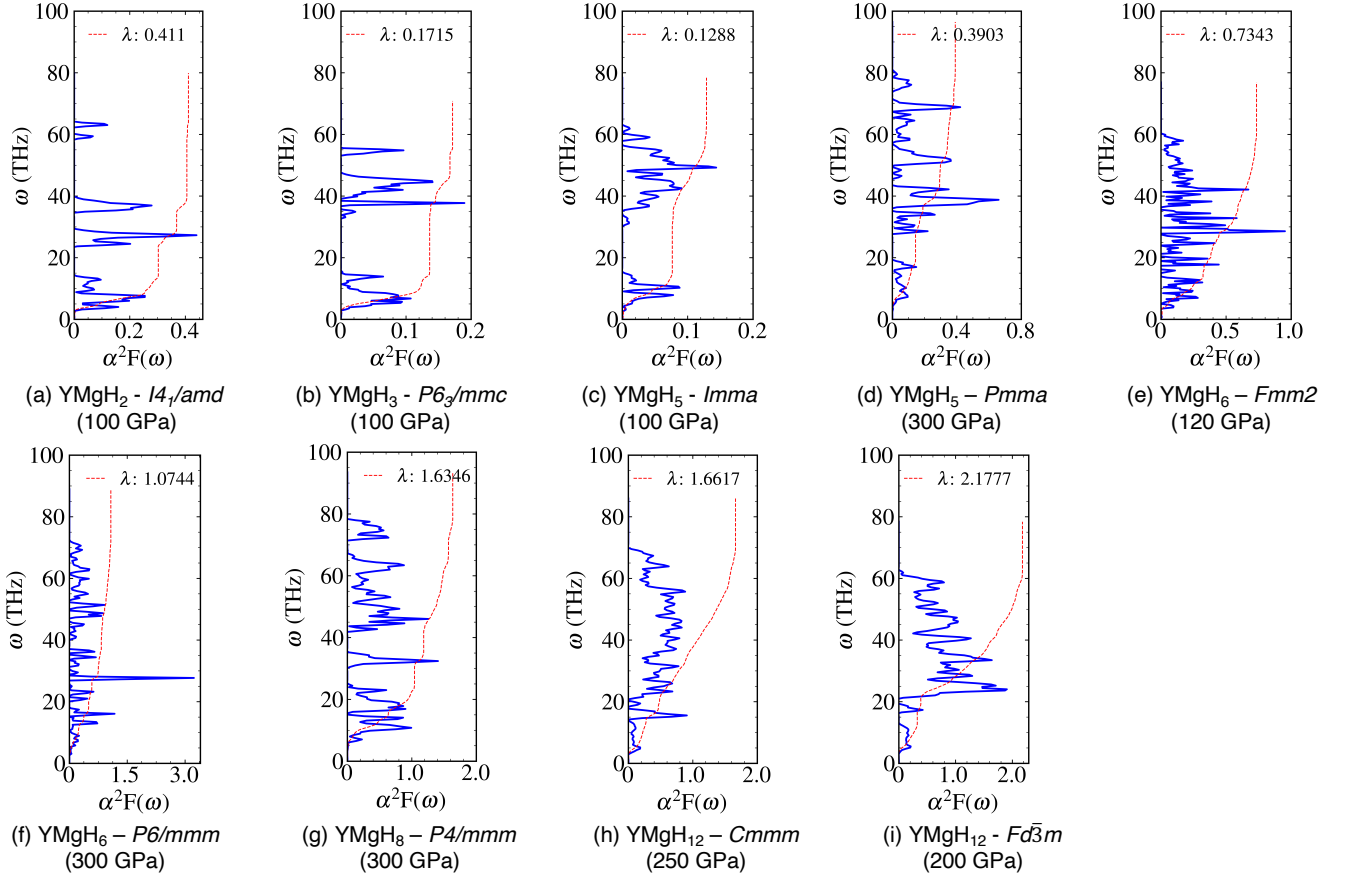


FIG. S6: Eliashberg spectral functions of (a) YMgH₂-*I4₁/amd* at 100 GPa, (b) YMgH₃-*P6₃/mmc* at 100 GPa, (c) YMgH₅-*Imma* at 100 GPa, (d) YMgH₅-*Pmma* at 300 GPa, (e) YMgH₆-*Fmm2* at 120 GPa, (f) YMgH₆-*P6/mmm* at 300 GPa, (g) YMgH₈-*P4/mmm* at 300 GPa, (h) YMgH₁₂-*Cmmm* at 250 GPa, and (i) YMgH₁₂-*Fd3m* at 200 GPa.

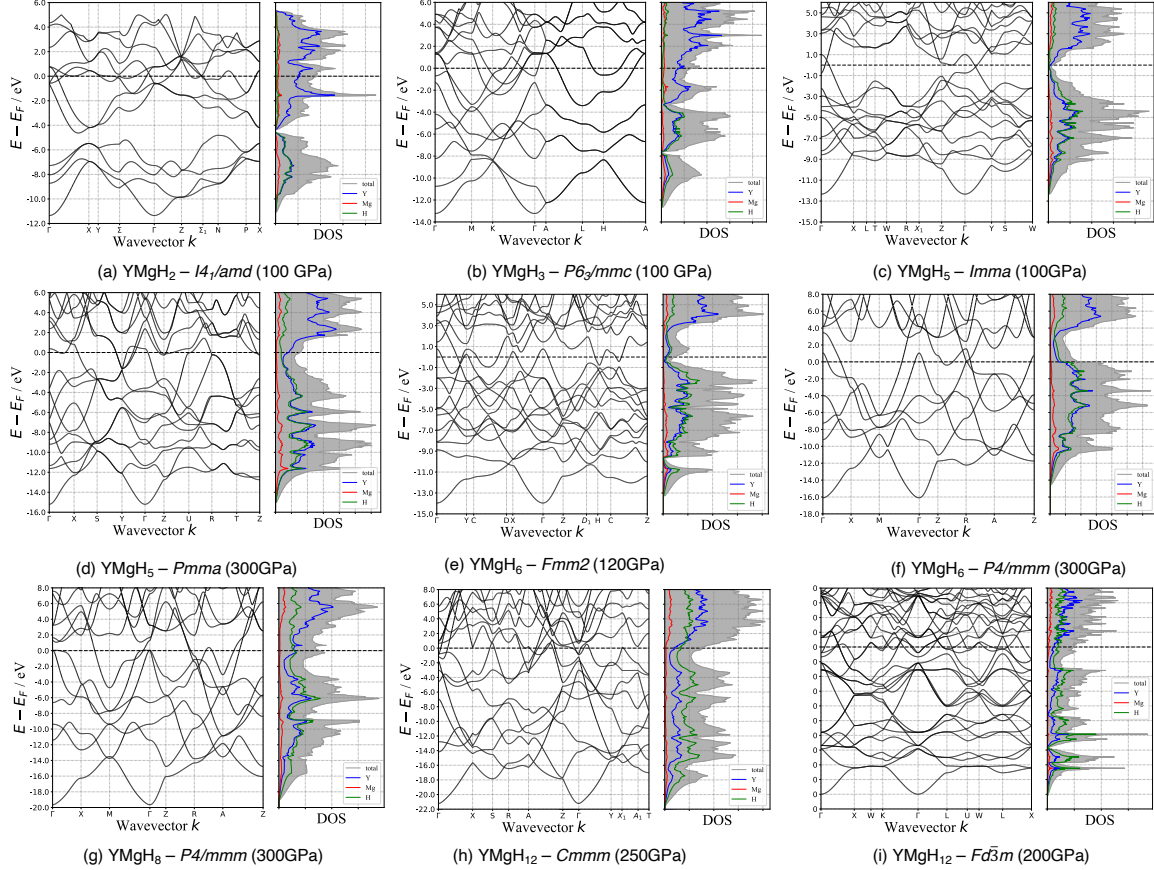


FIG. S7: Band structure and Density of state of the predicted YMgH_x phases.

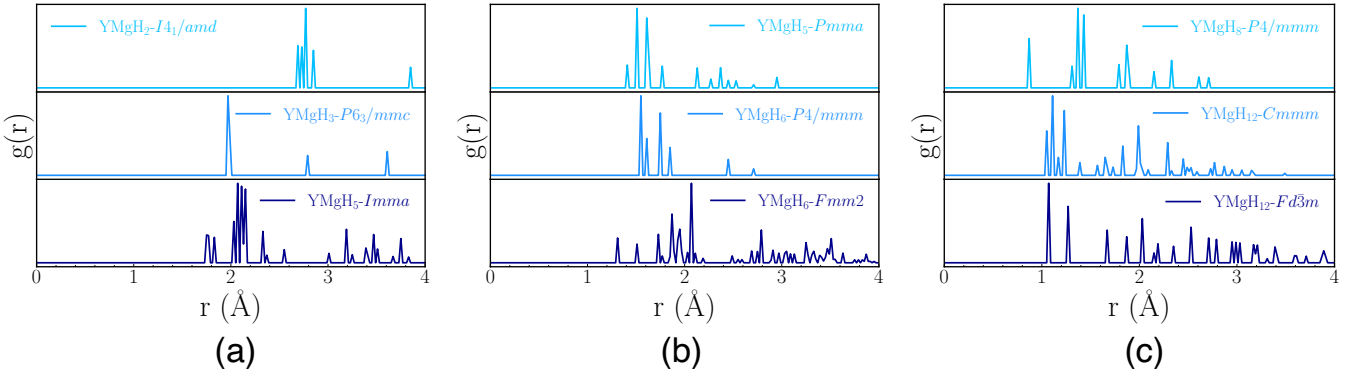


FIG. S8: The radial distribution function of the H-H atom pair in YMgH_x .

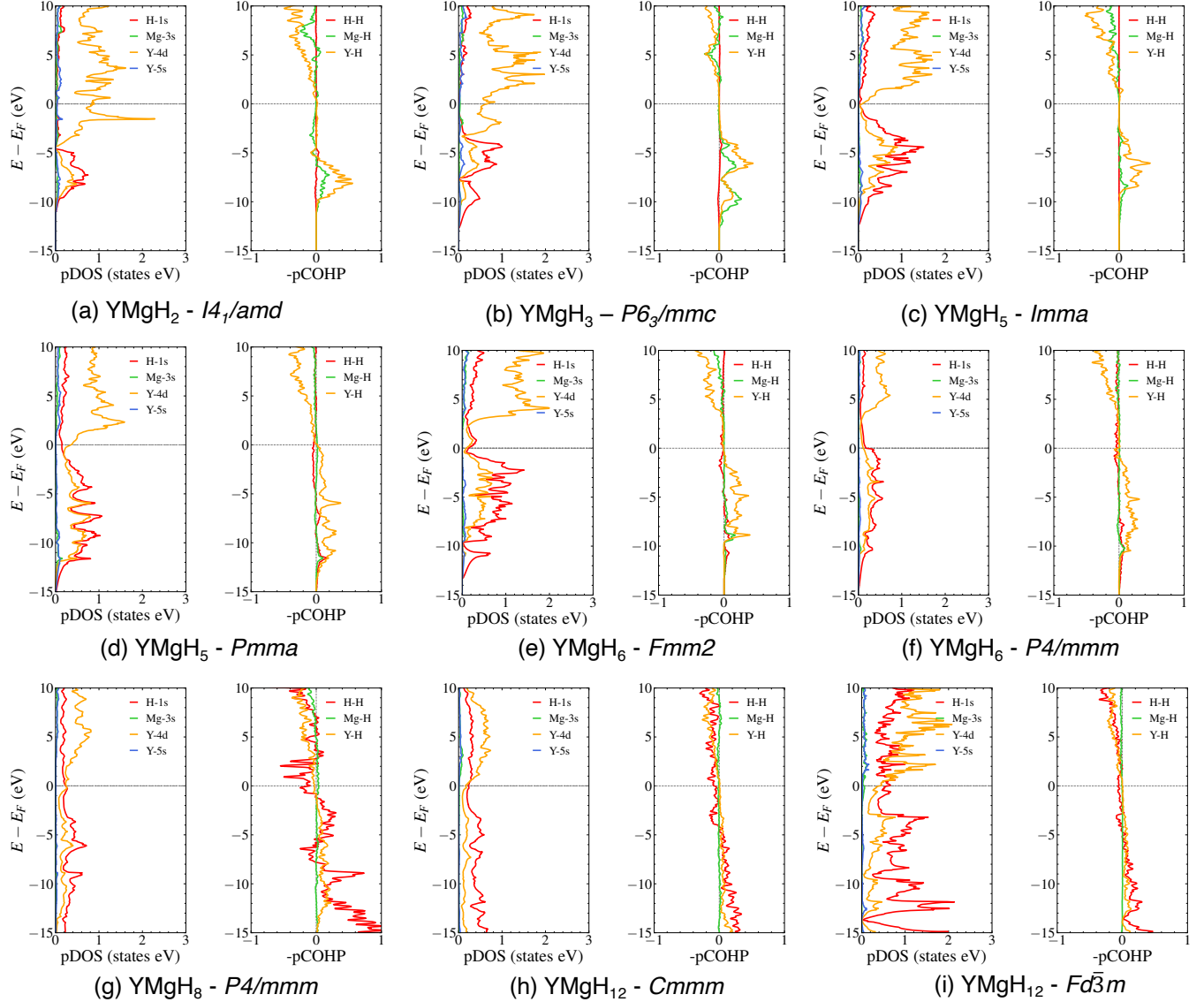


FIG. S9: The partial density of states (PDOS) and projected crystal orbital Hamilton population (pCOHP) of YMgH_x.

C. Supplementary tables

TABLE S2: The distances of the first nearest neighboring Y-H, Mg-H, and H-H atom pairs.

	YMgH ₂	YMgH ₃	YMgH ₅	YMgH ₅	YMgH ₆	YMgH ₆	YMgH ₈	YMgH ₁₂	YMgH ₁₂
Space group	<i>I4₁/amd</i>	<i>P6₃/mmc</i>	<i>Imma</i>	<i>Pmma</i>	<i>Fmm2</i>	<i>P4/mmm</i>	<i>P4/mmm</i>	<i>Cmmm</i>	<i>Fd̄3m</i>
Pressure (GPa)	100	100	100	300	120	300	300	250	200
Y-H	1.931	2.028	1.904	1.728	1.899	1.758	1.821	1.879	1.965
Mg-H	1.922	1.7035	1.652	1.562	1.677	1.540	1.584	1.726	1.834
H-H	2.681	1.971	1.778	1.517	1.725	1.540	0.864	1.040	1.097

TABLE S3: T_c estimated by McMillan formula using *ab initio* phonon calculations for YMgH_x at each pressure. λ and ω_{\log} are the parameters appearing in the formula.

Compound	Space group	<i>P</i> (GPa)	λ	ω_{\log} (K)	N_{E_F} (states/eV/Å ³)	T_c (K) at $\mu = 0.1 - 0.13$
YMgH ₂	<i>I4₁/amd</i>	100	0.411	451.20	0.0292	2.20 – 1.01
YMgH ₃	<i>P6₃/mmc</i>	100	0.1715	469.93	0.0200	$\ll 0.001$
YMgH ₅	<i>Imma</i>	100	0.1288	761.1124	0.0046	$\ll 0.001$
YMgH ₅	<i>Pmma</i>	200	0.4247	1036.858	0.0121	6.02 – 2.92
		300	0.3903	1219.4306	0.0141	4.44 – 1.83
YMgH ₆	<i>Fmm2</i>	120	0.7343	800.4893	0.0093	31.17 – 24.39
YMgH ₆	<i>P4/mmm</i>	300	1.0744	963.2549	0.0210	74.55 – 64.91
YMgH ₈	<i>P4/mmm</i>	300	1.6346	1012.8135	0.0249	124.77 – 114.70
YMgH ₁₂	<i>Cmmm</i>	250	1.6617	1224.0843	0.0209	152.92 – 140.78
		300	1.3054	1449.2025	0.0211	143.19 – 128.52
YMgH ₁₂	<i>Fd̄3m</i>	200	2.1777	1249.5972	0.0248	190.01 – 178.22
		300	1.8107	1408.7617	0.0271	188.55 – 174.78

TABLE S4: Crystal structures of Y-Mg-H predicted at each pressure (*P*). Lattice parameters (*a*, *b* and *c*) are given in unit of Å.

Compound	Space group	<i>P</i> (GPa)	Lattice parameters		Atomic coordinates (fractional)			
			Atoms		<i>x</i>	<i>y</i>	<i>z</i>	
YMgH ₂	<i>I4₁/amd</i>	100	<i>a</i> = <i>b</i> = 3.8598	Y(4 <i>b</i>)	0.00000	0.00000	0.50000	
			<i>c</i> = 7.9269	Mg(4 <i>a</i>)	0.00000	0.00000	0.00000	
			$\alpha = \beta = \gamma = 90^\circ$	H(8 <i>e</i>)	0.00000	0.00000	0.24241	
YMgH ₃	<i>P6₁/mmc</i>	100	<i>a</i> = <i>b</i> = 2.95056	Y(2 <i>a</i>)	0.00000	0.00000	0.00000	
			<i>c</i> = 8.36345	Mg(2 <i>d</i>)	0.33333	0.66667	0.75000	
			$\alpha = \beta = 90^\circ$	H(4 <i>f</i>)	0.33333	0.66667	0.36848	
			$\gamma = 120^\circ$	H(2 <i>b</i>)	0.00000	0.00000	0.25000	
YMgH ₄	<i>Pmn2₁</i>	100	<i>a</i> = 3.0249	Y(2 <i>a</i>)	0.00000	0.50190	0.48731	
			<i>b</i> = 4.0812	Mg(2 <i>a</i>)	0.00000	0.01506	0.81030	
			<i>c</i> = 5.5122	H(2 <i>a</i>)	0.00000	0.00618	0.48454	
			$\alpha = \beta = \gamma = 90^\circ$	H(2 <i>a</i>)	0.00000	0.23584	0.14577	
				H(2 <i>a</i>)	0.00000	0.59877	0.81387	
				H(2 <i>a</i>)	0.00000	0.75436	0.16581	
YMgH ₅	<i>Imma</i>	100	<i>a</i> = 3.5536	Y(4 <i>a</i>)	0.00000	0.00000	0.00000	
			<i>b</i> = 8.3654	Mg(4 <i>e</i>)	0.00000	0.25000	0.50640	
			<i>c</i> = 4.9179	H(8 <i>h</i>)	0.00000	0.07060	0.36745	
			$\alpha = \beta = \gamma = 90^\circ$	H(8 <i>g</i>)	0.25000	0.14083	0.75000	
				H(4 <i>e</i>)	0.00000	0.25000	0.09003	
YMgH ₅	<i>Pmma</i>	200	<i>a</i> = 3.6996	Y(2 <i>e</i>)	0.25000	0.00000	0.29815	
			<i>b</i> = 3.4314	Mg(2 <i>f</i>)	0.25000	0.50000	0.80204	

Continued on next page

TABLE S4 – continued from previous page

Compound	Space group	P (GPa)	Lattice parameters	Atomic coordinates (fractional)		
				Atoms	x	y
			$c = 4.5078$	H(4g)	0.00000	0.21208
			$\alpha = \beta = \gamma = 90^\circ$	H(2d)	0.00000	0.50000
				H(2e)	0.25000	0.00000
				H(2f)	0.25000	0.50000
					0.72445	0.18862
YMgH ₆	<i>F</i> _{mm2}	100	$a = 5.8175$	Y(8d)	0.24964	0.00000
			$b = 5.9495$	Mg(8c)	0.00000	0.24126
			$c = 8.7087$	H(8c)	0.00000	0.24353
			$\alpha = \beta = \gamma = 90^\circ$	H(8d)	0.18399	0.00000
				H(8b)	0.25000	0.25000
				H(8b)	0.25000	0.25000
				H(4a)	0.00000	0.00000
				H(4a)	0.00000	0.00000
				H(4a)	0.00000	0.00000
				H(4a)	0.00000	0.55987
				H(4a)	0.00000	0.00000
					0.77059	
YMgH ₆	<i>P</i> 4/ <i>mmm</i>	300	$a = 2.6235$	Y(1b)	0.00000	0.00000
			$b = 2.6235$	Mg(1c)	0.50000	0.50000
			$c = 3.9533$	H(4i)	0.00000	0.50000
			$\alpha = \beta = \gamma = 90^\circ$	H(1a)	0.00000	0.00000
				H(1d)	0.50000	0.50000
YMgH ₇	<i>P</i> 2/ <i>m</i>	150	$a = 2.8255$	Y(1e)	0.50000	0.50000
			$b = 2.8664$	Mg(1c)	0.00000	0.00000
			$c = 4.3458$	H(2n)	0.00699	0.50000
			$\alpha = \gamma = 90^\circ$	H(2n)	0.38478	0.50000
			$\beta = 90.8145^\circ$	H(2m)	0.49818	0.00000
				H(1a)	0.00000	0.00000
YMgH ₈	<i>P</i> 4/ <i>mmm</i>	300	$a = 2.5271$	Y(1a)	0.00000	0.00000
			$b = 2.5271$	Mg(1d)	0.50000	0.50000
			$c = 4.5369$	H(4i)	0.00000	0.50000
			$\alpha = \beta = \gamma = 90^\circ$	H(2g)	0.00000	0.00000
				H(2h)	0.50000	0.50000
YMgH ₉	<i>P</i> 2 ₁ / <i>m</i>	100	$a = 5.1702$	Y(2e)	0.41530	0.75000
			$b = 3.0745$	Mg(2e)	0.07454	0.75000
			$c = 5.4932$	H(4f)	0.08755	0.61229
			$\alpha = \gamma = 90^\circ$	H(2e)	0.06687	0.75000
			$\beta = 90.1008^\circ$	H(2e)	0.20436	0.25000
				H(2e)	0.20888	0.25000
				H(2e)	0.24539	0.25000
				H(2e)	0.26150	0.25000
				H(2e)	0.38701	0.75000
				H(2e)	0.42098	0.75000
					0.61655	0.91256
YMgH ₁₂	<i>C</i> _{mmm}	250	$a = 3.3296$	Y(2a)	0.00000	0.00000
			$b = 4.6364$	Mg(2c)	0.50000	0.50000
			$c = 4.6931$	H(8n)	0.12525	0.38836
			$\alpha = \beta = \gamma = 90^\circ$	H(8n)	0.38787	0.14919
				H(8m)	0.25000	0.28656
YMgH ₁₂	<i>F</i> _d ³ <i>m</i>	250	$a = b = c = 6.6105$	Y(8a)	0.00000	0.00000
			$\alpha = \beta = \gamma = 90^\circ$	Mg(8b)	0.00000	0.00000
				H(96h)	0.00934	0.12500
					0.24066	

-
- ¹ C. W. Glass, A. R. Oganov, and N. Hansen, *Comput. Phys. Commun.* **175**, 713 (2006).
- ² G. Kresse and J. Hafner, *Phys. Rev. B* **47**, 558 (1993).
- ³ G. Kresse and J. Hafner, *Phys. Rev. B* **49**, 14251 (1994).
- ⁴ G. Kresse and J. Furthmüller, *Comput. Mater. Sci.* **6**, 15 (1996).
- ⁵ G. Kresse and J. Furthmüller, *Phys. Rev. B* **54**, 11169 (1996).
- ⁶ J. P. Perdew, K. Burke, and M. Ernzerhof, *Phys. Rev. Lett.* **77**, 3865 (1996).
- ⁷ S. Maintz, V. L. Deringer, A. L. Tchougréeff, and R. Dronskowski, *J. Comput. Chem.* **37**, 1030 (2016).
- ⁸ A. Togo and I. Tanaka, *Scripta Mater.* **108**, 1 (2015).
- ⁹ P. Giannozzi, S. Baroni, N. Bonini, M. Calandra, R. Car, C. Cavazzoni, D. Ceresoli, G. L. Chiarotti, M. Cococcioni, I. Dabo, A. D. Corso, S. de Gironcoli, S. Fabris, G. Fratesi, R. Gebauer, U. Gerstmann, C. Gouguassis, A. Kokalj, M. Lazzeri, L. Martin-Samos, N. Marzari, F. Mauri, R. Mazzarello, S. Paolini, A. Pasquarello, L. Paulatto, C. Sbraccia, S. Scandolo, G. Sclauzero, A. P. Seitsonen, A. Smogunov, P. Umari, and R. M. Wentzcovitch, *J. Phys.: Condens. Matter* **21**, 395502 (2009).
- ¹⁰ P. Giannozzi, O. Andreussi, T. Brumme, O. Bunau, M. B. Nardelli, M. Calandra, R. Car, C. Cavazzoni, D. Ceresoli, M. Cococcioni, N. Colonna, I. Carnimeo, A. D. Corso, S. de Gironcoli, P. Delugas, R. A. DiStasio, A. Ferretti, A. Floris, G. Fratesi, G. Fugallo, R. Gebauer, U. Gerstmann, F. Giustino, T. Gorni, J. Jia, M. Kawamura, H.-Y. Ko, A. Kokalj, E. Küçükbenli, M. Lazzeri, M. Marsili, N. Marzari, F. Mauri, N. L. Nguyen, H.-V. Nguyen, A. O. de-la Roza, L. Paulatto, S. Poncé, D. Rocca, R. Sabatini, B. Santra, M. Schlipf, A. P. Seitsonen, A. Smogunov, I. Timrov, T. Thonhauser, P. Umari, N. Vast, X. Wu, and S. Baroni, *J. Phys.: Condens. Matter* **29**, 465901 (2017).
- ¹¹ P. Giannozzi, O. Baseggio, P. Bonfà, D. Brunato, R. Car, I. Carnimeo, C. Cavazzoni, S. de Gironcoli, P. Delugas, F. F. Ruffino, A. Ferretti, N. Marzari, I. Timrov, A. Urzu, and S. Baroni, *J. Chem. Phys.* **152**, 154105 (2020).
- ¹² W. L. McMillan, *Phys. Rev.* **167**, 331 (1968).
- ¹³ C. J. Pickard and R. J. Needs, *Nature Phys.* **3**, 473 (2007).
- ¹⁴ Q. Liu, C. Fan, and R. Zhang, *J. Appl. Phys.* **105**, 123505 (2009).
- ¹⁵ D. C. Lonie, J. Hooper, B. Altintas, and E. Zurek, *Phys. Rev. B* **87**, 054107 (2013).
- ¹⁶ H. Liu, I. I. Naumov, R. Hoffmann, N. W. Ashcroft, and R. J. Hemley, *Proc. Natl. Acad. Sci. USA* **114**, 6990 (2017).